EXTREME VACUUM TECHNOLOGY (BELOW 10^{-13} TORR) INCLUDING A PRESSURE CALIBRATION STUDY

QUARTERLY STATUS REPORT NO. 6
1 August - 1 November 1964

Contract NASr-63(06)

MRI Project No. 2675-P

For

Headquarters
National Aeronautics and Space Administration
Washington, D. C. 20546

MRI   MIDWEST RESEARCH INSTITUTE
425 VOLKER BOULEVARD/KANSAS CITY, MISSOURI 64110/AC 816 LO 1-0202

EXTREME VACUUM TECHNOLOGY (BELOW 10^{-13} TORR)
INCLUDING A PRESSURE CALIBRATION STUDY

by

Paul J. Bryant
Charles M. Gosselin
William Longley

QUARTERLY STATUS REPORT NO. 6
1 August - 1 November 1964

Contract NASr-63(06)

MRI Project No. 2675-P

For

Headquarters
National Aeronautics and Space Administration
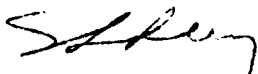Washington, D. C. 20546

A study of several phases of vacuum science and technology form the subject matter of this program. The characteristics of some ultra-high vacuum gauges, the analysis of various pumping mechanisms, and improved vapor jet pump design, cryogenic adsorption predictions, and cold welding studies are included.

Mr. George Wise of the NASA Lewis Research Laboratories in Cleveland, Ohio, is the technical monitor. This Quarterly Status Report covers the period from 1 August to 1 November 1964.

The research program is conducted in the Physics Section of Midwest Research Institute under the direction of Dr. Sheldon L. Levy and Mr. Gordon E. Gross. Dr. Paul J. Bryant serves as the principal investigator. Mr. Charles Gosselin and Dr. William Longley have conducted major portions of the research program.

Approved for:

MIDWEST RESEARCH INSTITUTE

Sheldon L. Levy, Director
Mathematics and Physics Division

4 December 1964

TABLE OF CONTENTS

SUMMARY

Several phases relating to the attainment and measurement of ultra-high vacuum are reported below. The phases covered are: response characteristics for Redhead and Kriesman gauges, determination of the gases present in UHV systems with oil diffusion and getter-ion pumping, the improvement of an adsorption calculation, the design of a dual expansion nozzle for vapor jet studies, the construction of a field emission microscope for UHV analysis, and initial operation of the extreme high vacuum system.

The response of magnetron gauges in their original form and with a cesiation treatment is reviewed. Numerous data have shown that a characteristic break from linearity and cutoff level exists for the magnetron gauges and that the pressure values at which these characteristics occur can be lowered by a cesiation treatment (see Section III-A below and NASA Report CR-84).

An analysis of the gas species present in a UHV system with getter-ion and oil diffusion pumping has shown many interesting comparisons. An important discovery was made regarding the operation of oil diffusion pump traps. A combined cryogenic and chemical trap has shown the ability to give more reliable and economical service.

The physical adsorption isotherm based on a triangular site model has been improved in several ways. The quantitative values originally computed from this isotherm were not in agreement with experimental values. However, there were questions regarding several of the input values so that the theory could not be immediately checked. One incorrect input value has now been discovered and corrected. This change will greatly improve the quantitative predictions from the theory. The improved theory is briefly summarized in Section III-C below; quantitative values will be computed and described in the next Summary Report.

A vapor nozzle with dual expansion chambers has been designed. Florescu's prediction regarding the operation of such a nozzle will be thoroughly tested with the vapor jet test apparatus (see NASA Report CR-84) and this new nozzle assembly. The opening or gap to the expansion chambers may be continuously varied during UHV operation of this test nozzle. Thus, a sufficient range of performance may be recorded to give a definitive analysis of this vapor jet design.

An electron field emission microscope has been constructed; some design and operational characteristics are discussed. The extreme high vacuum system, to which the microscope will be attached, is also discussed. Leak detection, degassing, and treatments to the electronics are described. An improved signal-to-noise level was required for the partial pressure analyzer to measure the low pressures in this system. A method for reducing the background leakage currents (and the origin of the currents) is described.

I. INTRODUCTION

The simulation of a given vacuum or known environment is required by many research programs. The investigation of physical or chemical interactions between materials requires that the materials be pure; that the surface be clean; or that the test environment be known and controlled. The required level of accuracy for these conditions is often greater than present technology provides, especially in the case of space simulation.

For example, a number of space simulation experiments specify a vacuum of 10^{-13} torr. The attainment of this pressure level appears to be within the ability of present technology. However, the measurement of 10^{-13} torr is questionable. Only a few intricate research instruments for pressure estimation are capable of operating in this range, while standard techniques and commercial equipment fail. Thus, the ability to measure a specified pressure of the level required for space simulation is at best uncertain. Present adsorption isotherm predictions for idealized conditions indicate, as mentioned above, that it should be possible to attain 10^{-13} torr or lower with liquid helium cryopumping techniques. However, the isotherms for vapor pressures vs. quantities of various gas species cryosorbed by a given panel material are not complete. Thus, the length of time over which a specified pressure can be maintained is also uncertain.

We may summarize this general introduction to the problems of simulating the vacuum of space by observing that both the measurement and maintenance of such low pressures are beyond the ability of standard technology. Some special techniques may be applied, but these research methods are still in the experimental stages. The development of several such areas of vacuum science and technology is described in this report.

II. EQUIPMENT AND TECHNIQUES

The design and construction of several research systems are described below. Included are a field emission microscope and a dual nozzle vapor jet. Several research techniques are described including a method for removing cesium poisoning with a hydrogen discharge.

A. Vapor-Jet Pumping Mechanism

A review of available literature on diffusion pump operations has suggested that previous analyses of the vapor-jet pumping mechanism have not been conclusive. The important problem here is to maintain high pumping speed when the vacuum system pressure is low. Florescu[1,2] suggests that both high jet speed and high concentration of working fluid are necessary to maintain good performance. On this basis, Alexander's[3] results are explained by stating that at high jet densities an appreciable rebounding of gas molecules was the limiting factor in pump speed, while a jet of low density does not work effectively at high speeds. In addition, fluid heating tends to increase concentration faster than it increases speed. Partly due to the increase in concentration and partly due to the relatively low speed, increased backspreading of the vapor occurs at high jet concentrations. Florescu performed some experiments on the increase of pump speed by diverting a portion of the working fluid into a strongly diverging nozzle. One question regarding the results is whether the limiting pressure for the system was due to desorption from unbaked walls or to backspreading of the vapor into the high vacuum side of the pump. Other experiments by Kennedy[4] suggest that random compression waves from eruptive boiling are an important source of backspreading, especially in baffled systems.

A new pump unit has been designed to test the Florescu prediction of higher rate of gas molecule removal by varying the vapor stream density. Figure 1 shows a partial cutaway of the new unit. For illustration, a Florescu-type nozzle is shown with a spoiler to divide the jet into two main streams, one with high expansion ratio and, hence, high velocity and low density; and the other with moderate expansion ratio and, hence, lower jet velocity and higher density. The system is designed so that jet caps can be replaced when the pump is removed from the vapor jet test apparatus (see Ref. 5). The main feature of the system is a linear motion feedthrough by which the nozzle gap can be varied while the pump is operating. This feedthrough consists of the following units: a shaft to which the cap is attached; a section of thin wall stainless steel tubing in which thermocouples can be inserted to determine temperatures in the vapor column and the mercury boiler; a bellows assembly at the bottom of the boiler to permit vertical displacement of the tube; a square shaft and square hole bushing to reduce the danger of twisting the bellows assembly; and a threaded shaft through a "micrometer" dial to indicate the nozzle gap.

1/   Florescu, N. A., _Australian J. Appl. Sci._, 8, 305 (1957).

2/   Florescu, N. A., _Vacuum_, 10, 250 (1960).

3/   Alexander, P., _J. Sci. Instr._, 23, 11 (1946).

4/   Kennedy, P. B., _1961 Trans. of the Eighth Vacuum Symposium and Second International Congress_, 320, Pergamon Press (1962).

5/   Bryant, P. J., C. M. Gosselin, and L. H. Taylor, NASA Contractor's Report CR-84, pp. 6-19, July 1964.
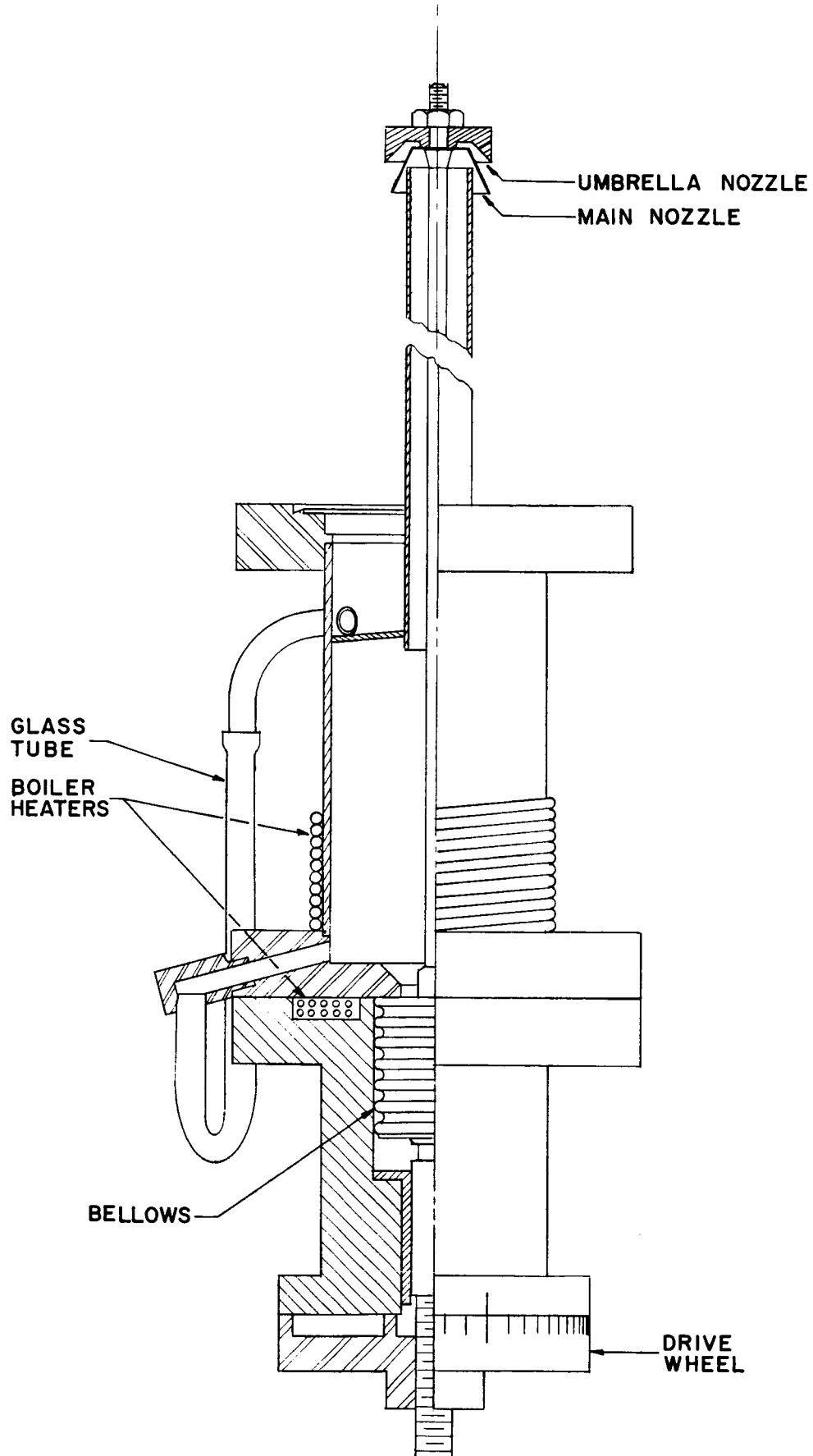
Fig. 1 - Test apparatus for experimental diffusion pump nozzles. A nozzle
with dual expansion chambers is shown. The drive mechanism pro-
vides for continuous variation of nozzle gap during operation.

Both heater tapes and a ring heater are provided so that thermal gradients within the mercury can be controlled to reduce eruptive boiling. The nozzle gap can be varied to check the sensitivity of pump speed to nozzle spacing at a given boiler temperature. The present method of gap variation with a positive mechanical attachment will avoid the blow-off problem encountered with the pump assembly described in Ref. 5. The interchangeability of caps on this system will permit future tests with various cap designs.

B. Field Emission Microscope

The electron field emission microscope was specially constructed by the Central Scientific Company according to the design given in the last Quarterly Report. Figure 2 shows the electronic control unit and microscope tube. Emission tip assemblies of both tungsten and platinum have also been constructed. The microscope will be used in direct conjunction with the sensitive partial pressure analyzer for adsorption studies and gas pressure observations.

The microscope tube is constructed of pyrex glass and stainless steel. A housekeeper's type glass to metal seal is incorporated for use in liquid nitrogen. This seal does not employ the usual kovar metal to graded glass connection. The pyrex glass is sealed directly to a stainless steel tube which has been reduced to a thin wall in the vicinity of the seal. Variations of thermal expansion between the glass and metal may be accommodated by the thin wall stainless tube over a wide temperature range. The microscope tube will be exposed to temperatures from 450°C to -195°C for bake-out and liquid nitrogen operation.

Magnification values available with the present tip arrangements are from one to five million times. Higher magnifications could easily be attained, but lower values were chosen so that the microscope could be used most effectively in the ultra-high vacuum range. The lower magnification arrangement serves to display a larger area of the tip on the viewing screen. After preliminary experiments are completed, the magnification will be reduced to 100,000 times so that 10^{-8} cm^2 of the metal tip surface may be observed.

The control unit shown in Fig. 2 provides a high voltage supply for electron emission and a filament current supply for degassing the tip. The high voltage source is continuously variable from zero to 5,000 v. with positive ground for safety. That is, the conductive coating on the glass microscope tube is attached to ground (through the metal flange) and serves as a grounded anode. The metal tip which is safely isolated from the metal flange may be driven as low as 5,000 v. below ground.
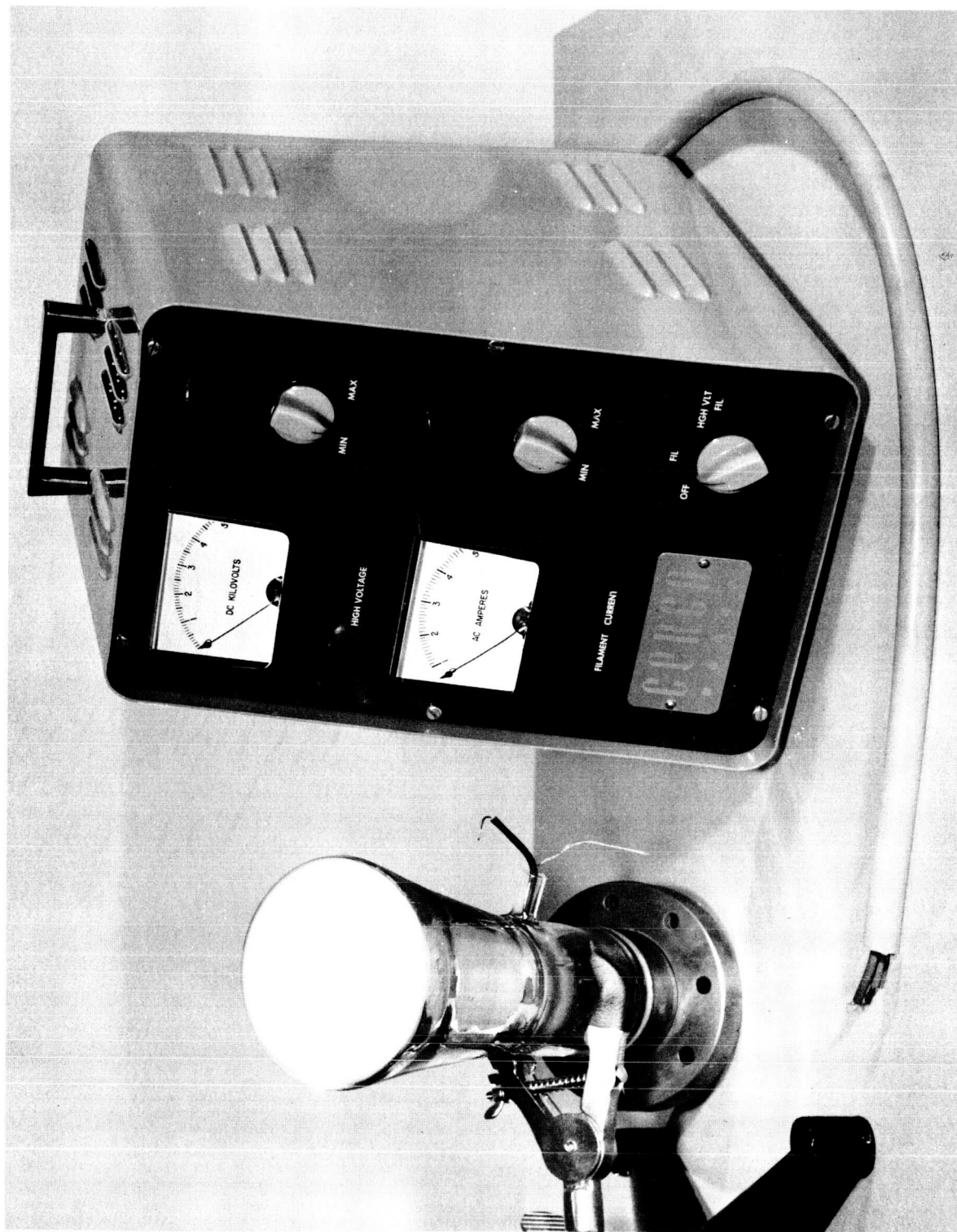
Fig. 2 - Electron field emission microscope tube and power supply. The glass tube is mounted directly (by means of the 4 in. O.D. Conflat Flange) onto the ionization chamber of a sensitive partial pressure analyzer. The 5 kv. high voltage provides the 10⁸ v/cm for field emission; the filament current provides thermal degassing of the tip.

Contaminants on the metal tip may be removed by selectively heating the tip holder. The variable filament current supply is provided for this purpose. Since this later power supply is well isolated from ground it is possible to float it on the negative 5,000 v. output, thus giving the combined ability to degass the tip while operating the microscope. Observation of the degassing process will be particularly interesting and useful.

C. Preparation of the Extreme High Vacuum System

The vacuum system (NASA, G-1769) which was described in the last report[6] has been prepared for low pressure operation. Initial leak detection and degassing cycles have been completed. The sensitivity of the gas analyzer was raised along with a net gain of the signal to noise ratio by a cesiation treatment. An increase of the electronic background occurred due to a cesium poisoning. Several remedies for this problem were examined and a hydrogen reduction method was found to be successful. Each of these preparatory processes is described in more detail below.

The vacuum system was baked at $400°C$ for several days. The temperature of the analyzer was raised to $417°C$ so that a portion of the cesium nitrate, which had been placed in the ion detector chamber, would decompose. The cesium liberated during this process reacts with the dynode surfaces of the ion detector. The addition of cesium to the dynodes lowers the work function of their surfaces and thus raises the output signal of the detector for a given input signal. Following the bake cycle, the tungsten filaments in the ion gauge and in the ion source of the analyzer were outgassed for one week. The system was then cooled to room temperature. The pressure as indicated by an ion gauge was in the low 10^{-9} torr range.

The 10^{-9} torr measurement was not an indication of the system's ultimate pressure capability since at this point it was at room temperature and was further limited by the unbaked parts of the auxiliary pumping unit. The 15 l/sec ion pump and associated plumbing will be sealed off from the main system for lower pressure operation.

Before filling the 85 liter capacity dewar with liquid nitrogen, an attempt was made to analyze the gases in the system. However, the background current generated by the ion detector portion of the partial pressure analyzer was so high (10^{-7} amp) that no peaks could be distinguished from this residual

---

[6] Bryant, P. J., Quarterly Status Report No. 5, Contract NASr-63(06), August 1964.

current. It was determined that cesium compounds had formed low resistance paths across the surfaces of the insulators in the ion detector.

Several techniques were tried in an attempt to eliminate the conductive paths. First, a tesla coil was employed in an effort to break down the paths by a high voltage discharge along the insulators. Evaporation of the cesium compounds was attempted by baking for 72 hr. at 250°C. Neither of these two methods was successful. A third technique involving the chemical activity of hydrogen was then tried.

The technique based on a reduction of the cesium compounds in a hydrogen discharge was successfully employed. Pure hydrogen gas was admitted to a pressure of 10^{-2} torr by means of a nickel diffuser. A high pressure (up to 1 torr) ion gauge* was also used. During the diffuser operation period a 2,500 v. potential was maintained across the ten dynodes of the ion detector (or about 250 v. across each pair of dynodes). The background current, including leakage currents in the detector, was monitored. This residual current decreased steadily to about 10^{-10} amp. A hydrogen gas discharge was then established within the system. The detector was operated in this gaseous discharge for 3 min. The diffuser was turned off and the system was pumped down to the 10^{-8} torr range. The background current was then 1.5×10^{-12} amp. which represented a decrease of five orders of magnitude due to the hydrogen discharge technique.

The extreme high vacuum system is now ready for a gas analysis and an ultimate pressure determination. The system will then be ready for regular operation. Periodically, the sensitivity of the electron multiplier (ion detector) will decline and require a reactivation with cesium. Following several reactivation cycles the cesium poisoning problem will recur. The hydrogen reduction technique described above will then be reapplied. Special techniques, such as described above, are necessary for operation in the extreme high vacuum range.

III. RESULTS AND CONCLUSIONS

Results from three research phases are presented below. Some results from a detailed study of magnetron type vacuum gauges are given. The results of a series of gas analyses in UHV systems are reported as a function of the type of pumping employed and the mechanism of trapping used. The discovery of

---

* A Varian Millitorr gauge.

an improved trap for use with oil diffusion pumps is reported. An improved physical adsorption isotherm is summarized. Recent corrections give promise for improved quantitative predictions with this theory.

A. Response of Magnetron Type Vacuum Gauges

The previous summary report[7] described the development of methods to analyze and to alter the response of magnetron type vacuum gauges. Since that time, a large quantity of data have been recorded and several new characteristics have been determined.

The characteristics of magnetron gauges were determined by means of a conductance regulated flow method (see Fig. 3). Standard triode ionization gauges were used to establish the value of conductance between the reference and test gauge positions. A magnetron gauge was then placed in the test position and a range of pressure values was covered by varying the flow rate of helium gas from the vycor glass diffuser. (The helium from this source is pure to a level of parts per million.) Helium was employed because the low boiling point and chemically inert nature gave assurance that the UHV pump would be the only gas sink in the system. Thus, the pressure ratio remains constant for values within the molecular flow range, which are of interest in this study of gauges.

Figure 4, gives an indication of the improvement which cesiation effects upon the response of magnetron gauges. The average non-cesiated gauge deviates from a linear response at a pressure of 7×10^{-10} torr and falls approximately one order of magnitude below linearity for a pressure of 2×10^{-11} torr, as shown in Fig. 4. A cesiated gauge, with a moderate sensitivity rise of two times, goes into the nonlinear region at one-half of the previous value or 3.5×10^{-10} torr and follows a response line of different slope so that it is in error by only 2.5 times (rather than 10 times) for the same pressure value of 2×10^{-11} torr.

The characteristics which have been observed for magnetron gauges may be outlined as follows: (1) the break from linear response occurs consistently at the same value of ion current for various gauges; (2) the nonlinear response is different for various gauge tubes; and (3) a lower limit for operation of the magnetron (i.e., a cutoff level) exists.

7/ Ibid.,Ref. 5, pp. 56-60.

MAGNETRON AND ION GAUGE COMPARISONS
BY A
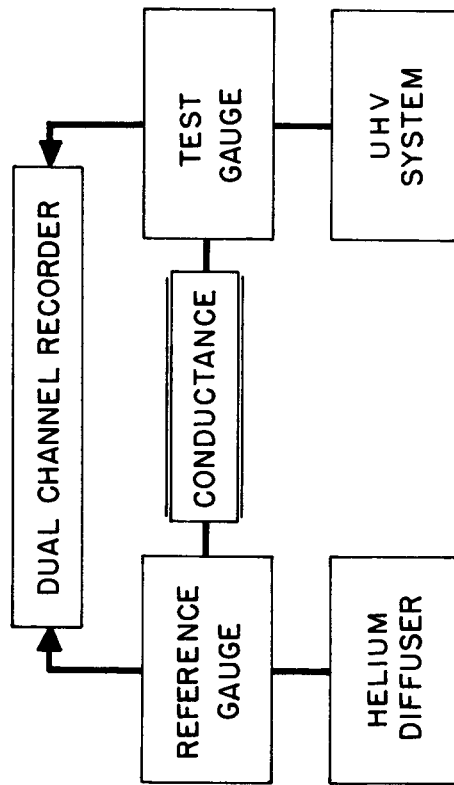## CONDUCTANCE REGULATED FLOW METHOD

Fig. 3 - A standard method for gauge comparisons was employed. The system is shown in block diagram above and described on page 9 of the text. A glass system with mercury diffusion pumps was used to maintain a uniform flow of helium gas for pressures throughout the UHV range. The non-uniform helium flow rates which may occur in helium cryopumped systems was thus avoided.
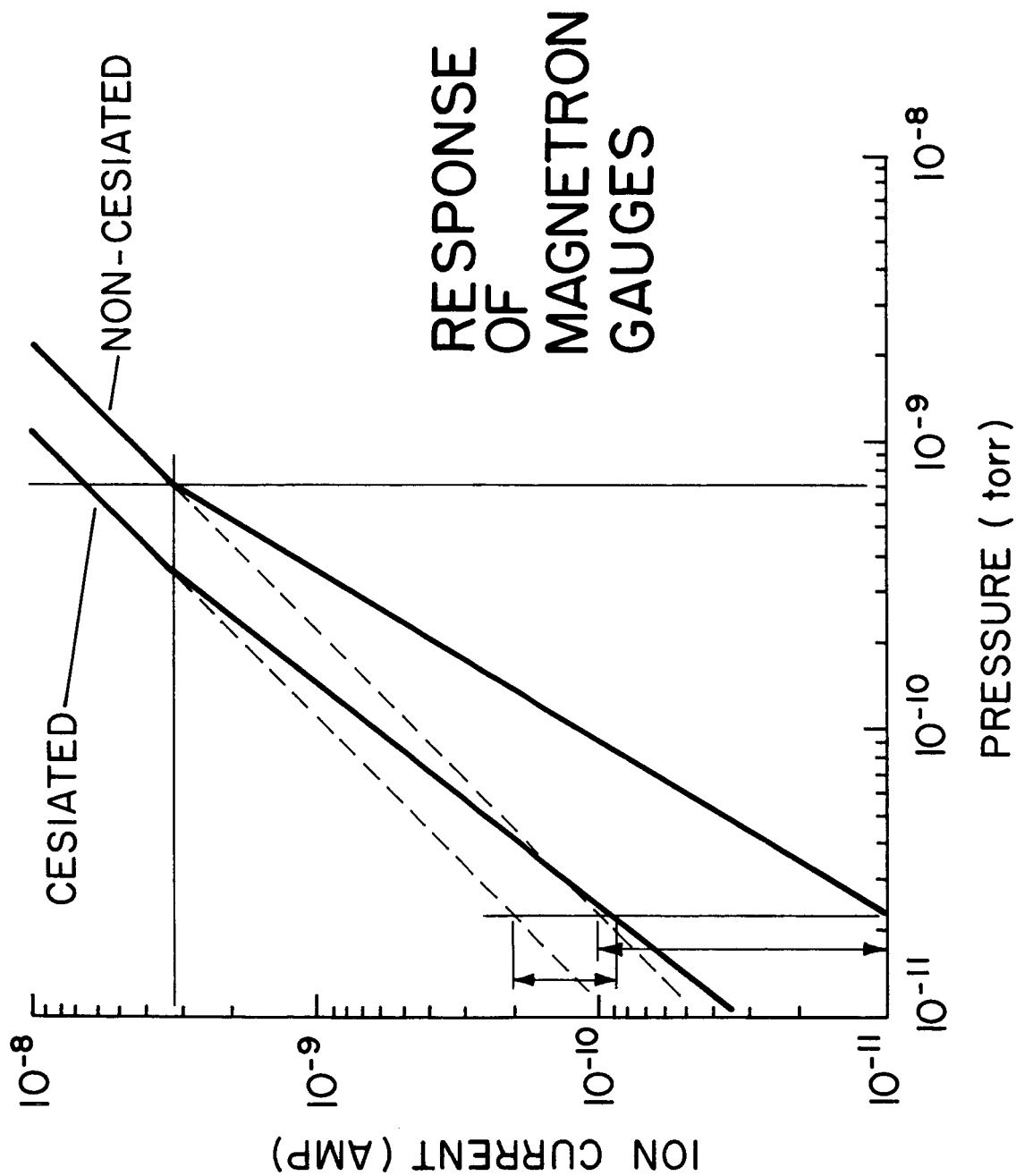
Fig. 4 - The response of a magnetron gauge may be increased by a cesium treatment. The example shown indicates only a moderate rise of two times. For a true pressure of 2.2×10^{-11} torr the average non-cesiated gauge reads 2.2×10^{-12} torr while the cesiated gauge reads 1.0×10^{-11} torr. Thus, an error of 10 times is reduced to 2.2 times.

The characteristics which result from a cesiation treatment of magnetron gauges may be summarized as follows: (1) the ion current to pressure response is raised (i.e., a sensitivity rise); (2) the nonlinear response of various tubes is raised and stabilized at one value; and (3) cutoff occurs at a lower corresponding pressure.

These observed characteristics are indicative of the fundamental process by which the magnetron operates. Each response mode corresponds to a mode of the discharge. The cesiation results were very useful as indicators of the problems involved when a magnetron is employed as a gauge. Cesiation also improved the response of the gauges in the linear range by increasing sensitivity and in the nonlinear range by lessening the divergence from linearity and by sustaining the discharge to a lower pressure.

The results outlined above were obtained with Redhead cold cathode magnetron gauges. A collection of all the data obtained with normal and cesiated Redhead gauges will be included in the forthcoming Summary Report.

Some preliminary results have been obtained with the Kriesman cold cathode discharge gauge. The data show a similarity to the general response characteristics of magnetron gauges. However, the break from linearity and decay to cutoff occurred at considerably higher pressures for the Kriesman gauge than for the Redhead gauge. Additional analyses are now being conducted.

B. Analysis of a Vacuum System with Both Oil Diffusion and Getter-Ion Pumping

The residual gases above a chemically trapped oil diffusion pump have been determined. The diffusion pump, special chemical trap, and partial pressure analyzer used in this work have been described earlier.[8] DC-705 silicone oil was chosen as the diffusion pump fluid. Preceding the gas analysis, the PPA system, the chemical trap and the plumbing connecting the trap to the inlet of the diffusion pump were baked to 400°C. The total pressure in the system was from 1 to 2 x 10^{-9} torr. The background total pressure in the PPA system (ion pumped and isolated from diffusion pump by a valve) was from 5 to 8 x 10^{-10} torr.

The species and amounts of the residual gases were determined to be a function of the temperature of the chemical trap. The predominant gases found in the system were H_2, CH_4, H_2O, CO, A, CO_2, and C_6H_6. Figure 5 displays the relative changes which occurred for the various test conditions.
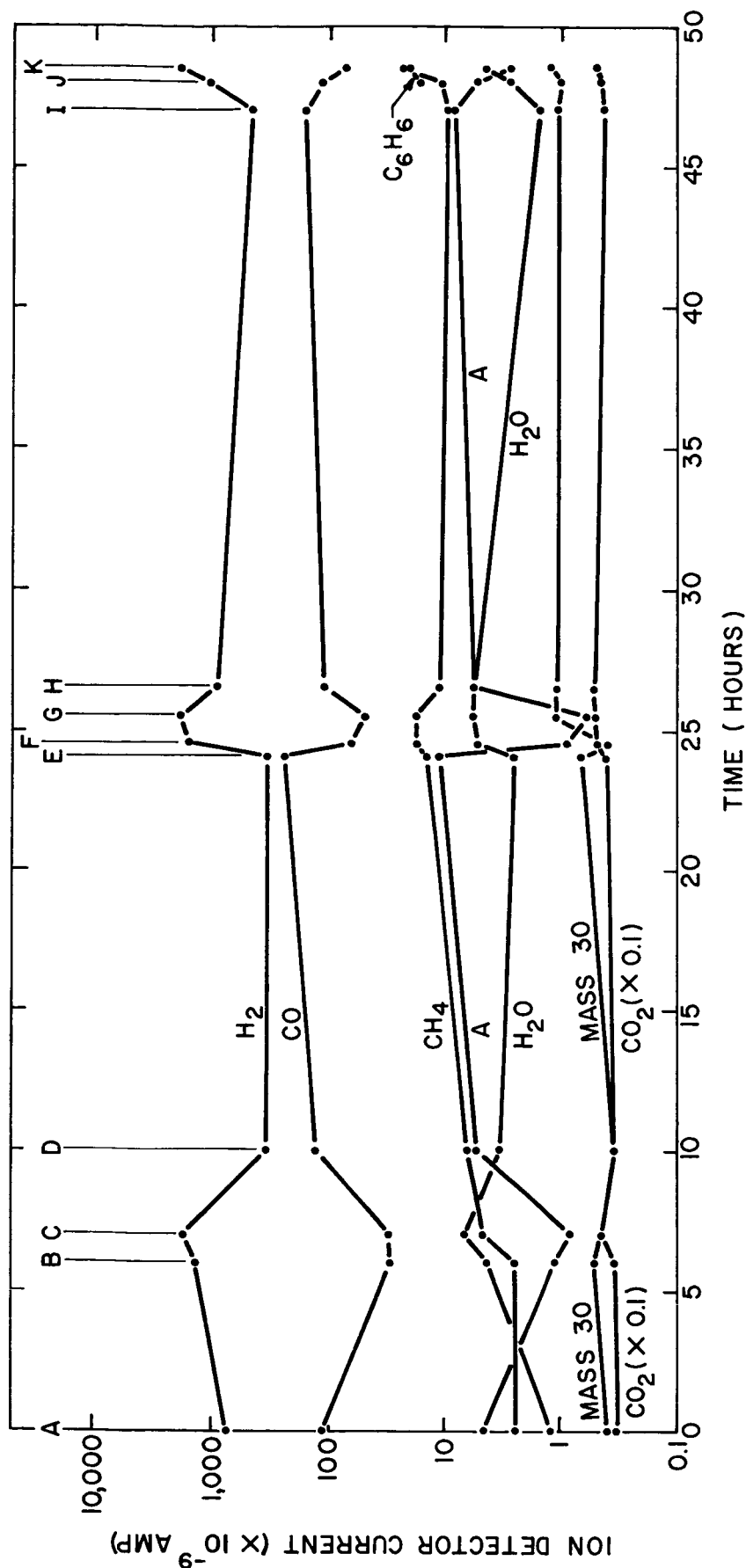
---

[8] Ibid., Ref. 5, pp. 20-29.

Fig. 5 - Comparison of the major residual gases in an UHV system for various pumping conditions.

Note: The following symbols define the conditions; IP = ion pump; DP = diffusion pump plus chemical trap; G = gettering action of ion pump when no voltage is applied; temperature of chemical trap; LN_2 = liquid nitrogen; DI&A = dry ice and acetone; Rm = room temperature; P_T = total pressure as determined by a closed grid ion gauge.

Conditions:

A. $P_T = 3.4 \times 10^{-10}$ torr	IP	
B. $P_T = 1.0 \times 10^{-9}$	IP + DP + LN_2	
C. $P_T = 1.4 \times 10^{-9}$	G + DP + LN_2	
D. $P_T = 5.1 \times 10^{-10}$	IP	
E. $P_T = 7.3 \times 10^{-10}$	IP	
F. $P_T = 1.2 \times 10^{-9}$	IP + DP + DI&A	
G. $P_T = 1.5 \times 10^{-9}$	G + DP + DI&A	
H. $P_T = 8.3 \times 10^{-10}$	IP	
I. $P_T = 5.5 \times 10^{-10}$	IP	
J. $P_T = 1.6 \times 10^{-9}$	IP + DP + Rm	
K. $P_T = 2.0 \times 10^{-9}$	G + DP + Rm	

ION DETECTOR CURRENT (X 10^{-9} AMP)

TIME (HOURS)

H_2, CO, CH_4, A, H_2O, MASS 30, CO_2 (X 0.1), C_6H_6

The carbon monoxide and argon peaks were determined to be strongly influenced by the 8 l/sec ion pump which is in the PPA system. The amount of these two gases was much less when the diffusion pump was operating.

The mass 30 peak showed a significant rise as the operating temperature of the trap increased. The increasing peak at mass 30 along with masses 25, 26, 27, and 29 (not shown) very likely indicated a buildup of ethane (C_2H_6) in the system. However, because of the small signal to noise ratio for these peaks, additional data must be processed in order to substantiate this conclusion (i.e., the presence of C_2H_6).

The cracking pattern for benzene is one of the characteristic patterns observed for DC-705 oil. However, C_6H_6 was not detected until the system was operated with the chemical trap at room temperature. This series of experiments has also shown that there is very little difference in the residual gases present in the system when the trap temperature was either -195°C or -80°C. These experiments show that chemical traps cooled to -80°C by mechanical refrigeration or CO_2 would have essentially the same efficiency as would traps operated at liquid nitrogen temperature. This discovery is important for the efficient and economical operation of oil diffusion pumped systems. The maintenance of liquid nitrogen traps has long been a problem. Fluctuation of the nitrogen level or loss of the coolant during a long term experiment has often nullified the experimental results. Mechanical refrigeration is a more reliable source of coolant. The results of this program have shown that chemical traps cooled to moderate temperature are as effective as liquid nitrogen traps. Therefore, this new more reliable means of trapping should prove to be very useful for vacuum systems employing oil diffusion pumps.

The analysis of mass spectrometer data is a time-consuming process. Therefore, a study is being conducted to determine the feasibility of using a computer to assist in the processing of relatively large amounts of data. With such a program many gas cracking pattern spectra could be analyzed for each experimental condition. Therefore, enough data could be processed so that statistical averages would be calculated in a relatively short time. Note that statistical averaging is highly desirable when working in regions where the signal to noise ratio is low; e.g., errors due to spurious peaks or electronic anomalies would be greatly reduced.

C. A Physical Adsorption Isotherm for Inert Gases

The physical adsorption isotherm theory developed earlier[9] has been revised by improving the energy expressions for the monolayers adsorbed. The

---

9/ Ibid.,Ref. 5, pp. 30-55.

triangular site model, shown in Fig. 6, is used in preference to the BET linear model. The effect of the introduction of an energy which is dependent on adsorbed particle interactions and an improved treatment of nearest neighbor interactions on the mathematical expressions is shown.

When the dependence of the energy of a particle in one layer of adsorbed gas on the presence of all other layers present is included in the energy constraint equation (Subsection (A) of Ref. 9), the relation becomes

$$dE = \sum_{j=1}^{\infty} \epsilon_{gj} \, dn_{gj} - \sum_{j=1}^{M} E_j \, dX_j = 0 \ , \tag{1}$$

where ϵ_{gj} is the energy of the jth energy level in the gas, n_{gj} is the number of gas particles occupying this level, E is the total energy of the system, X_j is the number of particles in the rth adsorbed layer, there are M adsorbed layers which have nonzero occupation numbers, and E_j is the effective adsorption energy. The effective adsorption energy is defined in terms of the energy of adsorption for a particle in the jth layer, W_j , and the coverage of the jth layer, θ_j , by the expression

$$E_j = W_j + \sum_{i=1}^{M} \theta_i \frac{dW_i}{d\theta_j} \ . \tag{2}$$

The expression for γ_j from Eq. (21) Ref. 9, must be set equal to the expression

$$\gamma_j = \frac{Km^{3/2}T^{5/2}}{p} e^{-E_j/k_o t} \ , \tag{3}$$

where p is the pressure, m is the mass of a gas particle, T is the absolute temperature, k_o is the Boltzmann constant, and K is a function of physical constants explicitly indicated in Eq. (52) of Ref. 9.

Fig. 7 - The extended geometry is shown according to the triangular site model. Nearest neighbor, next nearest neighbor, and interlayer distances are shown. The critical dependence on the parameter D is seen here since D represents the high binding energy region of first monolayer spacing.
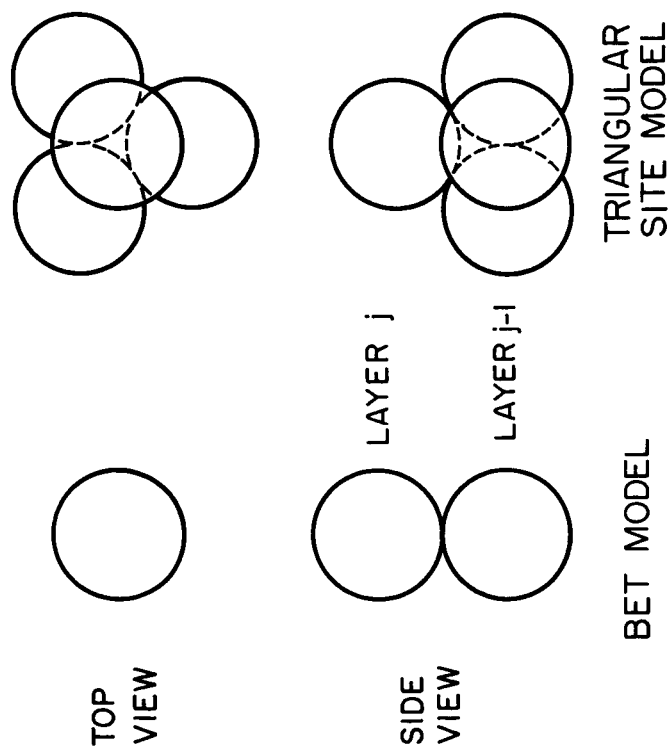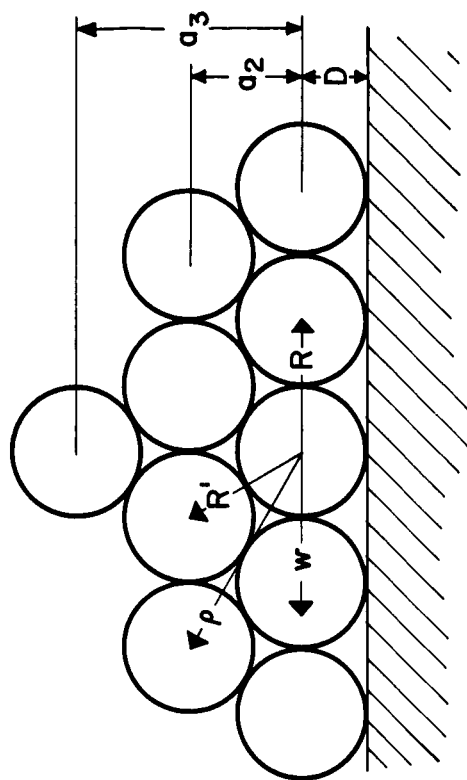

Fig. 6 - Site models, showing the geometric arrangement of atomic adsorption which is assumed for the development of the BET theory and for the present theory based on a triangular array.

- 16 -

The energy of adsorption for a particle in the jth layer is still treated as a sum of an adsorbate energy and the interaction energy with all other adsorbed particles. Although the numerical calculations are based on a Lennard-Jones (6-12) potential, the expressions for the energy are no longer based on an (n-2n) potential, but on a general potential with an attractive $-n^{th}$ power portion and a repulsive $-m^{th}$ power portion. We still retain the requirement that the attractive potential power be greater than 3. The following expressions give the adsorbent contribution to the energy of adsorption:

$$W_s = 2\pi \, \epsilon_I \, N_o D^3 \left(\frac{k}{\ell-2}\right)^{\frac{k}{k-\ell}} \left(\frac{k-2}{\ell}\right)^{\frac{\ell}{k-\ell}} \frac{1}{(k-3)(\ell-3)} \quad , \tag{4}$$

$$W_{sj} = \frac{W_s}{k-\ell} \left[\frac{k-3}{(1+d_j)^{\ell-3}} - \frac{\ell-3}{(1+d_j)^{k-3}} \right] \quad , \tag{5}$$

where ϵ_I is the maximum attractive energy in the $(\ell-k)$ curve for the interaction between one gas particle and one atom from the adsorbate, D is the equilibrium distance between the centers of the particles adsorbed in the first layer and a representative surface, N_o is the density of adsorbate molecules, and d_j is the distance between the plane of centers for layer j and the plane of centers for layer ℓ in units of D . Figure 7 shows D and $a_j = Dd_j$ as well as the dimensions used in the calculation of cooperative interaction of the adsorbed particles.

For adsorbed particles which are not nearest neighbors, the z-function developed earlier is still used, but it is generalized to an (n-m) potential,

$$z(r) = \frac{\pi \epsilon \sigma_o r^2}{m-n} \left(\frac{m^m}{n^n}\right)^{\frac{1}{m-n}} \left[\frac{1}{n-2}\left(\frac{\sigma}{r}\right)^n - \frac{1}{m-2}\left(\frac{\sigma}{r}\right)^m \right] \quad , \tag{6}$$

where ϵ is the maximum attractive energy between two particles, σ is the distance of closest approach, and σ_o is the number of adsorbed molecules per

unit area in a complete layer. If the ith layer has no sites with a nearest neighbor relation to the particle of the jth layer under consideration, it contributes an amount to W_j of W_{ij}, where

$$W_{ij} = \theta_i \, z(|a_i - a_j|) \quad . \tag{7}$$

Except for layer $j=1$, there is one layer in which three nearest neighbors are guaranteed, the $j-1$ layer, with a contribution

$$W_{j-1,j} = \theta_{j-1} z(\rho) - \frac{3}{2}\varphi(R') \quad , \tag{8}$$

where R' is the nearest neighbor distance for two layers and ρ is chosen to make $z(\rho)$ equal to the contribution from the next nearest neighbors in layer $j-1$. Now one has to consider the probability of nearest neighbors in the j and $j+1$ layers. A decent approximation to this probability can be obtained with the function P_j defined as follows:

$$P_j = \frac{\theta_{j+1}}{3 \, \theta_j^3} \, P_{j-1}^2 \quad , \qquad P_o = 3\theta_1 \quad . \tag{9}$$

By using this function, one can write the last two contributions to the cooperative energy as follows:

$$W_{j+1,j} = \theta_{j+1} \, z(\rho) - \frac{P_j}{2}\varphi(R') \quad , \tag{10}$$

$$W_{jj} = \theta_j z(w) + P_{j-1} \, \epsilon \quad , \tag{11}$$

where w is chosen to make $z(w)$ equal to the contribution from all second-nearest neighbor sites in the same layer.

The energy of adsorption can now be written

$$W_j = W_{sj} - \frac{1}{2}(3f'_j + P_j)\,\varphi(R') + P_{j-1}\epsilon + \theta_j z(w) + (f'_j \theta_{j-1} + \theta_{j+1})\,z(\rho)$$

$$+ \sum_{i=1}^{j-2} \theta_i z(a_j - a_i) + \sum_{i=j+2}^{M} \theta_i z(a_i - a_j) \quad , \tag{12}$$

where f'_j is one when j is not one and zero when j is one. The effective adsorption energy can be developed from Eqs. (2) and (12) and written as:

$$E_j = W_{sj} + 2 P_{j-1}\,\epsilon - \frac{1}{2}\left(3 + P_{j-1}\theta_{j-1}\big/\theta_j\right) f'_j\,\varphi(R') - \sum_{i=j+1}^{M} 2^{i-j-1}\theta_i$$

$$\left[P_{i-1}\epsilon - P_i\varphi(R')\right]\big/\theta_j + 2\,\theta_j\,z(w) + 2(f'_j\theta_{j-1} + \theta_{j+1})\,z(\rho)$$

$$+ 2\sum_{i=1}^{j-2} \theta_i\,z(a_j - a_i) + 2\sum_{i=j+2}^{M} \theta_i\,z(a_i - a_j) \quad . \tag{13}$$

Numerical values will be computed with this improved theory and included in the forthcoming Summary Report.